Separation of CO_2 from CH_4 Using Mixed-Ligand Metal−Organic Frameworks

Youn-Sang Bae,[†] Karen L. Mulfort,[‡,§] Houston Frost,[†] Patrick Ryan,[†] Sudeep Punnathanam,[†] Linda J. Broadbelt,[†] Joseph T. Hupp,*[,‡] and Randall Q. Snurr*[,†]

Department of Chemical and Biological Engineering, Northwestern University, Evanston, Illinois 60208, Department of Chemistry, Northwestern University, Evanston, Illinois 60208, and The Chemical Sciences and Engineering Division, Argonne National Laboratory, Argonne, Illinois 60439

Received February 20, 2008. Revised Manuscript Received May 9, 2008

The adsorption of CO_2 and CH_4 in a mixed-ligand metal−organic framework (MOF) $Zn_2(NDC)_2(DPNI)$ [NDC = 2,6-naphthalenedicarboxylate, DPNI = *N*,*N*′-di-(4-pyridyl)-1,4,5,8-naphthalene tetracarboxydiimide] was investigated using volumetric adsorption measurements and grand canonical Monte Carlo (GCMC) simulations. The MOF was synthesized by two routes: first at 80 °C for two days with conventional heating, and second at 120 °C for 1 h using microwave heating. The two as-synthesized samples exhibit very similar powder X-ray diffraction patterns, but the evacuated samples show differences in nitrogen uptake. From the single-component CO_2 and CH_4 isotherms, mixture adsorption was predicted using the ideal adsorbed solution theory (IAST). The microwave sample shows a selectivity of ∼30 for CO_2 over CH_4, which is among the highest selectivities reported for this separation. The applicability of IAST to this system was demonstrated by performing GCMC simulations for both single-component and mixture adsorption.

1. Introduction

Carbon dioxide is often found as an impurity in natural gas and landfill gas, where methane is the major component. The presence of CO_2 reduces the energy content of natural gas and can lead to pipeline corrosion.[1–7] If natural gas meets established purity specifications, it is designated "pipeline quality methane," which increases its commercial value. To meet pipeline requirements, natural gas must comply with strict CO_2 concentration limits, as low as 2%.[1,2,5]

For the separation of CO_2 from natural gas, several technologies, such as absorption, cryogenic distillation, membrane separation, and adsorption, have been used. Among these technologies, adsorption-based methods such as pressure swing adsorption (PSA) are promising because of their simple and easy control, low operating and capital investment costs, and superior energy efficiency.[1,8,9] In particular, adsorption is advantageous for the case of medium- and small-size processes.[1,9] After the suggestion by Sircar in the late 1980s,[10] many studies have been performed on PSA processes for the separation and purification of CO_2 from gaseous streams containing CH_4.[1,3,4,11]

A key step in the design of PSA processes for the separation and purification of CO_2 is the selection of a highly selective adsorbent with a high CO_2 capacity.[1,8,9,11] Most studies of CO_2/CH_4 separation have focused on zeolites[1,2,6,12,13] and carbon-based adsorbents.[3,4,8,13,14] Recently, metal−organic frameworks (MOFs) have been recognized as a new family of porous materials that have potential applications in separations, sensing, gas storage, and catalysis.[15–17] MOFs consist of metal or metal-oxide corners connected by organic linkers. They are synthesized in a self-assembly process from these well-defined building blocks and have high porosity and well-defined pore sizes. The synthetic strategy opens up the possibility to systematically vary pore size and chemical functionality in the search for an optimal adsorbent. For separations, an additional advantage is that MOFs can be regenerated under milder conditions than most zeolites, which require considerable heating and the associated high costs.[18]

To date, most studies of adsorption in MOFs have focused on single-component gases, and little is known about mixture behavior even though understanding multicomponent adsorption equilibrium is essential for designing adsorption-based separation processes. For CO_2/CH_4 mixtures in MOFs, all of the published work to date has come from molecular simulation. Yang and Zhong used grand canonical Monte Carlo (GCMC) to simulate mixtures of CO_2 and CH_4 in Cu-BTC and MOF-5.[19,20] At 1 bar and 298 K, they predicted that Cu-BTC has a selectivity of about 6 for CO_2 over CH_4, and MOF-5 has a selectivity of about 2, independent of gas-phase composition. Babarao used GCMC simulations to compare CO_2/CH_4 mixtures in MOF-5, the zeolite silicalite, and C_{168} schwarzite.[13] They found that MOF-5 has a

* Author to whom correspondence should be addressed. E-mail: j-hupp@northwestern.edu (J.T.H.); snurr@northwestern.edu (R.Q.S.).
[†] Department of Chemical and Biological Engineering.
[‡] Department of Chemistry.
[§] Argonne National Laboratory.

(1) Cavenati, S.; Grande, C. A.; Rodrigues, A. E. *Energy Fuels* **2006**, *20*, 2648.
(2) Cavenati, S.; Grande, C. A.; Rodrigues, A. E. *J. Chem. Eng. Data* **2004**, *49*, 1095.
(3) Kim, M. B.; Bae, Y. S.; Choi, D. K.; Lee, C. H. *Ind. Eng. Chem. Res.* **2006**, *45*, 5050.
(4) Kapoor, A.; Yang, R. T. *Chem. Eng. Sci.* **1989**, *44*, 1723.
(5) Li, Y.; Chung, T. S.; Kulprathipanja, S. *AIChE J.* **2007**, *53*, 610.
(6) Li, P. Y.; Tezel, F. H. *Microporous Mesoporous Mater.* **2007**, *98*, 94.
(7) Li, S. G.; Falconer, J. L.; Noble, R. D. *J. Membr. Sci.* **2004**, *241*, 121.
(8) Peng, X.; Wang, W. C.; Xue, R. S.; Shen, Z. M. *AIChE J.* **2006**, *52*, 994.
(9) Yang, R. T. *Gas Separation by Adsorption Processes*; Butterworths: Boston, MA, 1987.
(10) Sircar, S. *Sep. Sci. Technol.* **1988**, *23*, 519.
(11) Yang, R. T. *Adsorbents: Fundamentals and Applications*; John Wiley & Sons, Inc.: Hoboken, NJ, 2003.
(12) Leyssale, J. M.; Papadopoulos, G. K.; Theodorou, D. N. *J. Phys. Chem. B* **2006**, *110*, 22742.
(13) Babarao, R.; Hu, Z. Q.; Jiang, J. W.; Chempath, S.; Sandler, S. I. *Langmuir* **2007**, *23*, 659.
(14) Goetz, V.; Pupier, O.; Guillot, A. *Adsorption* **2006**, *12*, 55.
(15) Snurr, R. Q.; Hupp, J. T.; Nguyen, S. T. *AIChE J.* **2004**, *50*, 1090.
(16) Rowsell, J. L. C.; Yaghi, O. M. *Angew. Chem., Int. Ed.* **2005**, *44*, 4670.
(17) Mueller, U.; Schubert, M.; Teich, F.; Puetter, H.; Schierle-Arndt, K.; Pastre, J. *J. Mater. Chem.* **2006**, *16*, 626.
(18) Surble, S.; Millange, F.; Serre, C.; Düren, T.; Latroche, M.; Bourrelly, S.; Llewellyn, P. L.; Ferey, G. *J. Am. Chem. Soc.* **2006**, *128*, 14889.
(19) Yang, Q. Y.; Zhong, C. L. *J. Phys. Chem. B* **2006**, *110*, 17776.
(20) Yang, Q. Y.; Zhong, C. L. *ChemPhysChem* **2006**, *7*, 1417.

10.1021/la800555x CCC: $40.75
Published on Web 07/11/2008

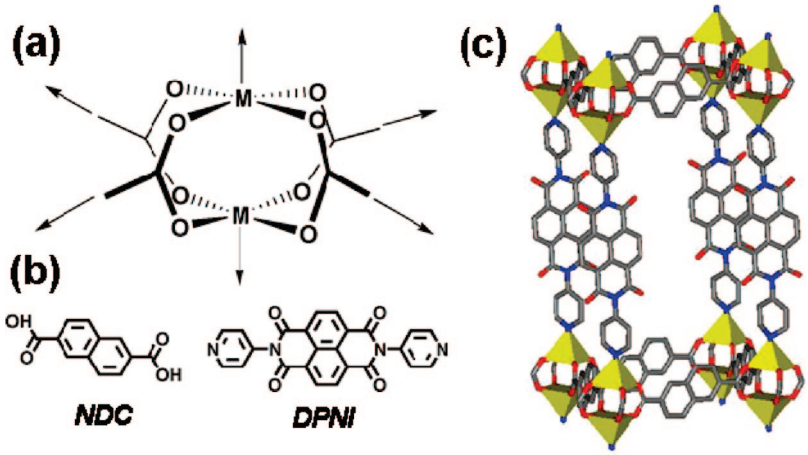

Figure 1. (a) Mixed-ligand paddlewheel coordination geometry (M = Zn). (b) Chemical structure of MOF ligands NDC and DPNI. (c) Single crystal structure of **1**. For clarity, hydrogens are omitted, and only one level of interpenetration is depicted. Gray represents carbon, blue nitrogen, red oxygen, and yellow polyhedra represent Zn clusters.

larger storage capacity, but the selectivity is similar in all three materials. Both groups report that the simulated mixture behavior matches well with the behavior calculated from single-component isotherms using the ideal adsorbed solution theory (IAST).[13,19,21]

In this work, we report results for CO_2/CH_4 mixture adsorption in a mixed-ligand paddlewheel MOF[22]using a combination of experimental measurements, IAST, and molecular simulation. Ma et al. previously reported a family of mixed-ligand MOFs that exhibit permanent microporosity.[22] As shown in Figure 1, these MOFs contain carboxylate-terminated linkers in two directions to define two-dimensional sheets that are pillared by pyridyl linkers in the third dimension. The use of two different linkers opens up more possibilities to tune pore size and chemical functionality independently. Because of the difficulties in measuring multicomponent adsorption,[23] we measured the single-component isotherms and calculated the mixture behavior using IAST. The IAST, originated by Myers and Prausnitz,[21] is a well-studied method to predict multicomponent isotherms from pure-gas isotherms. It has been shown to accurately predict gas mixture adsorption in many zeolites[13,24,25] and a few MOF materials.[13,19] The applicability of IAST to the mixed-ligand MOF was tested by performing single-component and mixture GCMC simulations. The simulated single-component isotherms were fed into IAST, and the predicted mixture behavior was compared with the mixture simulation results. Molecular simulations of adsorption isotherms in MOFs have generally shown good agreement with experiments.[19,20,26–29] Thus, differences between simulated and experimental isotherms can provide additional characterization for deviations of experimental MOF samples from the perfect crystalline structure.[30,31]

2. Experimental and Simulation Methods

2.1. Materials Synthesis and Characterization. The mixed-ligand MOF ($Zn_2(NDC)_2(DPNI)$), **1**, (NDC = 2,6-naphthalenedicarboxylate, DPNI = *N*,*N*′-di-(4-pyridyl)-1,4,5,8-naphthalene tetracarboxydiimide) was synthesized first by a conventional route (**1-C**) by heating for two days to effect slow crystallite growth.[22] We also prepared this material by a microwave-assisted method (**1-M**), which was shown previously to allow the rapid and efficient production of several IRMOFs with uniform crystal size.[32]

Commercial reagents were purchased from Sigma-Aldrich (ACS grade) and used as received unless otherwise noted. The syntheses of *N*,*N*′-di-(4-pyridyl)-1,4,5,8-naphthalenetetracarboxydiimide (DPNI) and **1-C** have previously been reported.[33,34] A sample preparation follows: $Zn(NO_3)_2 \cdot 6H_2O$ (600 mg, 2.0 mmol), H_2NDC (87 mg, 0.4 mmol), DPNI (170 mg, 0.4 mmol), and 200 mL of dimethylformamide (DMF) were added to a 500-mL flat-bottom flask. The flask was sonicated until all contents were dissolved and placed in an 80 °C oil bath for two days. The bright yellow crystalline product was removed from the flask, isolated via filtration, washed with DMF, and allowed to dry in air. $Zn_2(NDC)_2(DPNI)$ (**1-C**) recovered: 239 mg, 18% yield based on zinc. The microwave-assisted synthesis of **1** was carried out using an Initiator Microwave Synthesizer from Biotage. Slightly different conditions were discovered to yield **1** through microwave-assisted synthesis. It should be stressed that the exact same conditions (i.e., component ratio and temperature) were attempted and did not yield a pure phase of **1** by means of microwave heating. A sample preparation follows: $Zn(NO_3)_2 \cdot 6H_2O$ (600 mg, 2.0 mmol), H_2NDC (217 mg, 1.0 mmol), DPNI (214 mg, 0.5 mmol), and 200 mL of DMF were combined in a 250-mL Erlenmeyer flask. The flask was sonicated until all contents were dissolved. The solution was divided equally among 10 20-mL capacity microwave vials. Each vial was microwave heated without stirring at 120 °C for 1 h and allowed to stand overnight. The yellow microcrystalline powder was removed from each vial, isolated via filtration, washed with DMF, and allowed to dry in air. $Zn_2(NDC)_2(DPNI)$ (**1-M**) recovered: 362 mg, 27% yield based on zinc.

Powder X-ray diffraction (PXRD) patterns were recorded with a Rigaku XDS 2000 diffractometer using nickel-filtered Cu Kα radiation ($\lambda = 1.5418$ Å) over a range of $5° < 2\theta < 40°$ in 0.1° steps with a 1-s counting time per step. Powder samples were placed in the diffractometer mounted on a stainless steel holder with double-sided tape. Thermogravimetric analyses (TGAs) were performed on a Mettler-Toledo TGA/SDTA851e. Samples (3−5 mg) in alumina pans were heated from 25 to 700 °C at 10 °C/min under N_2. Nitrogen

(21) Myers, A. L.; Prausnitz, J. M. *AIChE J.* **1965**, *11*, 121.
(22) Ma, B. Q.; Mulfort, K. L.; Hupp, J. T. *Inorg. Chem.* **2005**, *44*, 4912.
(23) Talu, O. *Adv. Colloid Interface Sci.* **1998**, *76−77*, 227.
(24) Challa, S. R.; Sholl, D. S.; Johnson, J. K. *J. Chem. Phys.* **2002**, *116*, 814.
(25) Goj, A.; Sholl, D. S.; Akten, E. D.; Kohen, D. *J. Phys. Chem. B* **2002**, *106*, 8367.
(26) Düren, T.; Sarkisov, L.; Yaghi, O. M.; Snurr, R. Q. *Langmuir* **2004**, *20*, 2683.
(27) Garberoglio, G.; Skoulidas, A. I.; Johnson, J. K. *J. Phys. Chem. B* **2005**, *109*, 13094.
(28) Frost, H.; Düren, T.; Snurr, R. Q. *J. Phys. Chem. B* **2006**, *110*, 9565.
(29) Walton, K. S.; Millward, A. R.; Dubbeldam, D.; Frost, H.; Low, J. J.; Yaghi, O. M.; Snurr, R. Q. *J. Am. Chem. Soc.* **2008**, *130*, 406.
(30) Walton, K. S.; Snurr, R. Q. *J. Am. Chem. Soc.* **2007**, *129*, 8552.
(31) Düren, T.; Millange, F.; Ferey, G.; Walton, K. S.; Snurr, R. Q. *J. Phys. Chem. C* **2007**, *111*, 15350.
(32) Ni, Z.; Masel, R. I. *J. Am. Chem. Soc.* **2006**, *128*, 12394.
(33) Dinolfo, P. H.; Williams, M. E.; Stern, C. L.; Hupp, J. T. *J. Am. Chem. Soc.* **2004**, *126*, 12989.
(34) Mulfort, K. L.; Hupp, J. T. *J. Am. Chem. Soc.* **2007**, *129*, 9604.

adsorption isotherms were measured with an Autosorb 1-MP from Quantachrome Instruments. Samples of a known weight (35−50 mg) were loaded into a sample tube and evacuated at 110 °C under 10^{-5} Torr dynamic vacuum for 24 h. After evacuation, the sample and tube were precisely weighed again to obtain the evacuated sample weight. The Brunauer−Emmett−Teller (BET) surface area was determined in the range $0.007 < P/P_o < 0.05$ (see Supporting Information); the Dubinin−Raduskevich (DR) micropore volume was determined in the range $10^{-5} < P/P_o < 0.01$ since the micropores fill at very low relative pressures (see Supporting Information).

2.2. Adsorption Measurements. The adsorption isotherms of CO_2 and CH_4 on both samples were measured volumetrically at 296 K up to 18 atm (see Supporting Information). Before each measurement, a 40−60 mg sample was evacuated at 100 °C overnight, and the void volume of the system was determined by using He gas. CO_2 (99.9%) and CH_4 (99%) were obtained from Airgas, Inc. (Radnor, PA). Prior to analysis, gases were passed through molecular sieves to remove residual moisture. Equilibrium pressures were measured with an MKS Baratron transducer 627B (accuracy ± 0.12%). Adsorbate was dosed into the system incrementally, and equilibrium was assumed when no further change in pressure was observed (within 0.01 kPa).

2.3. GCMC Simulations. Carbon dioxide and methane adsorption was modeled using GCMC with a version of our multipurpose simulation code Music[35] modified to handle nonorthorhombic cells. The framework was considered rigid with coordinates from Ma et al.[22] The rigid framework and mobile CO_2 molecules were modeled atomistically, while methane was treated as a united atom sphere. Dispersion and repulsion interactions were modeled with a 12−6 Lennard-Jones potential between all atoms within a 12.8 Å cutoff. The Lennard-Jones parameters for the framework atoms were from the DREIDING force field.[36] Methane parameters were obtained from Goodbody et al.,[37] while CO_2 parameters came from the TraPPE potential.[38] This model places a Lennard-Jones center on each carbon and oxygen atom. Additionally, charges of −0.35, +0.70, and −0.35 are given to the oxygen, carbon, and oxygen, respectively, in order to represent the molecule's quadrupole moment. The C−O bond length is 1.16 Å, and the bond angle is 180 degrees. Lorentz−Berthelot mixing rules were employed to calculate the sorbate/framework and the CO_2/CH_4 Lennard-Jones parameters.

Partial charges for the MOF framework atoms were calculated with density functional theory (DFT) using the quantum chemical package Gaussian 03.[39] The exchange and correlation functional by Perdew, Burke, and Ernzerhof[40,41] was employed with a 6-31+G* basis set, which includes one diffuse and one polarization function on atoms heavier than He. The CHelpG method[42] was used to calculate charges from the DFT results with atomic radii obtained from Bondi.[43] Similar methods have been employed previously to estimate charges and binding energies in MOFs.[19,20,44–47] Representative clusters were chosen from the MOF framework for the DFT calculations. Each cluster consisted of one of the organic linker molecules coordinated to metal corner units on both ends. The metal corner was terminated with methyl or amine groups where the other organic linkers would normally exist. The clusters were used to provide atomic charges for both the organic units, as well as the metal corner. Ewald summation was used to calculate the electrostatic interactions in the GCMC simulations.

GCMC simulations were completed for single component isotherms of CO_2 and CH_4 separately, as well as for a variety of mixtures. The pure component and mixture fugacities needed as inputs to the simulations were calculated using the Peng−Robinson equation of state. The binary interaction parameter was assumed to be zero, as in previous work for CO_2 and CH_4 mixtures.[13] Each step in the Monte Carlo routine consisted of the insertion of a new molecule, deletion of an existing molecule, translation, or rotation of an existing molecule. A total of 10 million steps were used, the first 50% for equilibration and the last 50% to calculate the ensemble averages. Using the method of Myers and Monson,[48] excess adsorption isotherms were generated from the simulated (absolute) results in order to compare with experimental data. Further details about the simulations are provided in the Supporting Information.

3. Results and Discussion

3.1. Characterization. The crystal structure for the mixed-ligand MOF, $Zn_2(NDC)_2(DPNI)$ (**1-C**), synthesized by the conventional method has been reported previously.[22] The crystals from the microwave synthesis (**1-M**) were too small for single-crystal structure determination. Both as-synthesized materials (**1-C** and **1-M**) showed fairly uniform rectangular crystallites, but the crystal size of **1-M** (150 μm × 20 μm) was considerably smaller than that of **1-C** (400 μm × 150 μm). As shown in Figure 2, both as-synthesized materials gave powder X-ray patterns that closely match the simulated pattern, although **1-M** has noticeably weaker crystallinity and more line broadening than **1-C**. Also the relative intensities of low-angle peaks ($2\theta = 7-9°$) are weaker for **1-C** and **1-M** compared to the simulated PXRD pattern. In a recent paper, Hafizovic et al. reported that, for MOFs with a large void fraction, the intensities of the XRD reflections particularly at low 2θ are highly dependent on species present in the pores.[49] Hence, the differences in relative peak intensity of the low-angle peaks for **1-C** and **1-M** may indicate that the materials have some extra species in the pores, such as nonvolatile reactants, partial collapse, or higher levels of interpenetration.[49] The PXRD patterns of the materials evacuated at 110 °C overnight (**1-C′** and **1-M′**) show deviations from the as-synthesized materials. However, when these materials are resolvated in DMF, the PXRD patterns are converted back to the original patterns, indicating that the materials may be distorted during evacuation, but the crystallinity and the original structure are recovered upon resolvation. Similar reversible dynamic behavior has also been observed by others.[50–54]

The thermal stability of **1-C** and **1-M** was analyzed by TGA (see Supporting Information). For the TGA curves of the as-

(35) Gupta, A.; Chempath, S.; Sanborn, M. J.; Clark, L. A.; Snurr, R. Q. *Mol. Simul.* **2003**, *29*, 29.
(36) Mayo, S. L.; Olafson, B. D.; Goddard, W. A. *J. Phys. Chem.* **1990**, *94*, 8897.
(37) Goodbody, S. J.; Watanabe, K.; Macgowan, D.; Walton, J.; Quirke, N. *J. Chem. Soc., Faraday Trans.* **1991**, *87*, 1951.
(38) Potoff, J. J.; Siepmann, J. I. *AIChE J.* **2001**, *47*, 1676.
(39) Frisch, M. J.; Trucks, G. W.; Schlege, l. H. B.; Scuseria, G. E.; Robb, M. A.; Cheeseman, J. R.; Montgomery, J. A., Jr.; Vreven, T.; Kudin, K. N.; Burant, J. C.; Millam, J. M.; Iyengar, S. S.; Tomasi, J.; Barone, V.; Mennucci, B.; Cossi, M.; Scalmani, G.; Rega, N.; Petersson, G. A.; Nakatsuji, H.; Hada, M.; Ehara, M.; Toyota, K.; Fukuda, R.; Hasegawa, J.; Ishida, M.; Nakajima, T.; Honda, Y.; Kitao, O.; Nakai, H.; Klene, M.; Li, X.; Knox, J. E.; Hratchian, H. P.; Cross, J. B.; Adamo, C.; Jaramillo, J.; Gomperts, R.; Stratmann, R. E.; Yazyev, O.; Austin, A. J.; Cammi, R.; Pomelli, C.; Ochterski, J. W.; Ayala, P. Y.; Morokuma, K.; Voth, G. A.; Salvador, P.; Dannenberg, J. J.; Zakrzewski, V. G.; Dapprich, S.; Daniels, A. D.; Strain, M. C.; Farkas, O.; Malick, D. K.; Rabuck, A. D.; Raghavachari, K.; Foresman, J. B.; Ortiz, J. V.; Cui, Q.; Baboul, A. G.; Clifford, S.; Cioslowski, J.; Stefanov, B. B.; Liu, G.; Liashenko, A.; Piskorz, P.; Komaromi, I.; Martin, R. L.; Fox, D. J.; Keith, T.; Al-Laham, M. A.; Peng, C. Y.; Nanayakkara, A.; Challacombe, M.; Gill, P. M. W.; Johnson, B.; Chen, W.; Wong, M. W.; Gonzalez, C.; Pople, J. A. *Gaussian 03, Revision C.02*; Gaussian, Inc.: Wallingford, CT, 2004.
(40) Perdew, J. P.; Burke, K.; Ernzerhof, M. *Phys. Rev. Lett.* **1996**, *77*, 3865.
(41) Perdew, J. P.; Burke, K.; Ernzerhof, M. *Phys. Rev. Lett.* **1997**, *78*, 1396.
(42) Breneman, C. M.; Wiberg, K. B. *J. Comput. Chem.* **1990**, *11*, 361.
(43) Bondi, A. *J. Phys. Chem.* **1964**, *68*, 441.
(44) Sagara, T.; Klassen, J.; Ganz, E. *J. Chem. Phys.* **2004**, *121*, 12543.
(45) Mueller, T.; Ceder, G. *J. Phys. Chem. B* **2005**, *109*, 17974.
(46) Yang, Q. Y.; Zhong, C. L. *J. Phys. Chem. B* **2006**, *110*, 655.
(47) Nicholson, T. M.; Bhatia, S. K. *J. Phys. Chem. B* **2006**, *110*, 24834.
(48) Myers, A. L.; Monson, P. A. *Langmuir* **2002**, *18*, 10261.
(49) Hafizovic, J.; Bjorgen, M.; Olsbye, U.; Dietzel, P. D. C.; Bordiga, S.; Prestipino, C.; Lamberti, C.; Lillerud, K. P. *J. Am. Chem. Soc.* **2007**, *129*, 3612.
(50) Biradha, K.; Fujita, M. *Angew. Chem., Int. Ed.* **2002**, *41*, 3392.
(51) Maji, T. K.; Matsuda, R.; Kitagawa, S. *Nat. Mater.* **2007**, *6*, 142.
(52) Lee, E. Y.; Jang, S. Y.; Suh, M. P. *J. Am. Chem. Soc.* **2005**, *127*, 6374.
(53) Kitaura, R.; Seki, K.; Akiyama, G.; Kitagawa, S. *Angew. Chem., Int. Ed.* **2003**, *42*, 428.
(54) Zhao, X. B.; Xiao, B.; Fletcher, A. J.; Thomas, K. M.; Bradshaw, D.; Rosseinsky, M. J. *Science* **2004**, *306*, 1012.

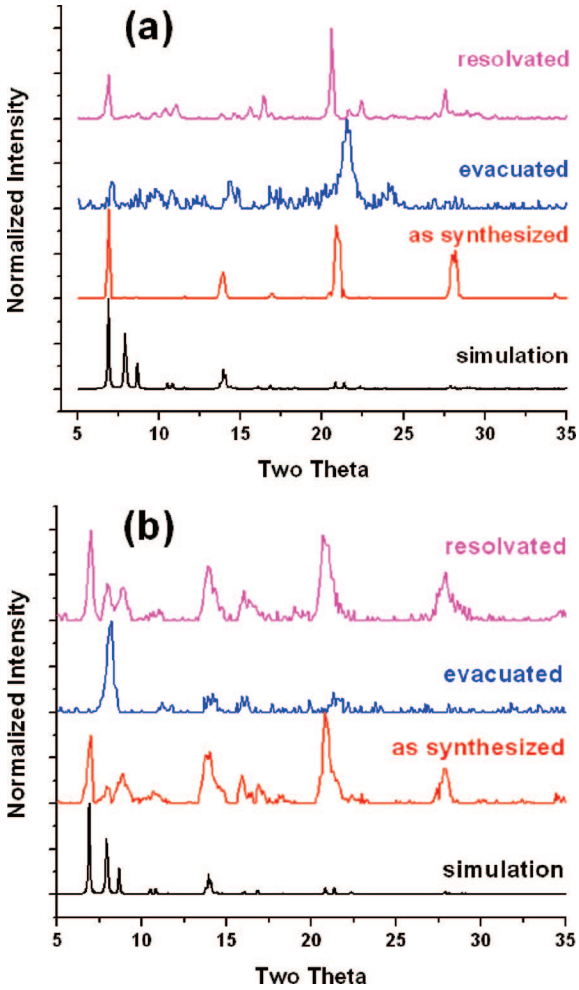

Figure 2. PXRD patterns for (a) **1-C** and (b) **1-M** for simulated, as-synthesized, evacuated, and resolvated samples.

synthesized materials, the initial mass loss between 70 and 200 °C (~30%) is consistent with the solvent loss expected from the single-crystal structural data (32.67%). This indicates that the pore volumes of both as-synthesized samples (**1-C** and **1-M**) match that of the perfect crystal. Moreover, the frameworks are stable until ~400 °C, where framework decomposition starts. TGA curves of **1-C′** and **1-M′** indicate that almost all guest solvent molecules in the framework are removed by evacuation at 110 °C under vacuum overnight.

Nitrogen adsorption and desorption isotherms at 77 K of the evacuated samples (**1-C′** and **1-M′**) are shown in Figure 3. On the basis of the TGA results, the pore volumes of the as-synthesized samples (**1-C** and **1-M**) are similar to each other and match very well with that of the perfect crystal structure. However, as shown in Figure 3, the adsorption capacities of N_2 at 77 K for the evacuated samples differ considerably from one another. The evacuated microwave sample (**1-M′**) has a much lower BET surface area and DR micropore volume than the conventional sample (**1-C′**) (see Table 1). Moreover, the BET surface area and micropore volume of **1-C′** are only half of that calculated geometrically from the perfect crystal structure. These differences may be due to pore contractions of the frameworks after evacuation. For both samples, N_2 adsorption/desorption isotherms show slight hysteresis, which has been observed in some flexible MOFs.[51,55,56]

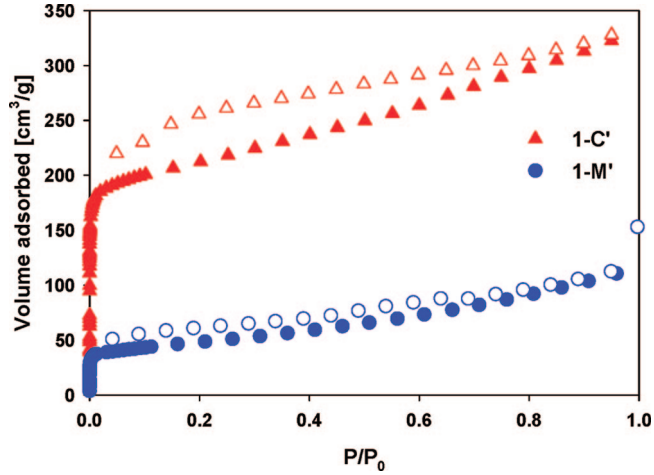

Figure 3. N_2 adsorption and desorption isotherms in **1-C′** and **1-M′** at 77 K. Closed symbols represent adsorption, open symbols represent desorption.

Table 1. BET Surface Area, Micropore Volume, and Pore Size for the Perfect Crystal and Evacuated Samples 1-C′ and 1-M′

sample	BET surface area (m^2/g)	micropore volume (cm^3/g)	pore size (Å)
perfect crystal[a]	1761	0.68	4.9/5.8
1-C′	802	0.34	5.0
1-M′	167	0.064	4.7

[a] Geometric calculations from the single-crystal structure.

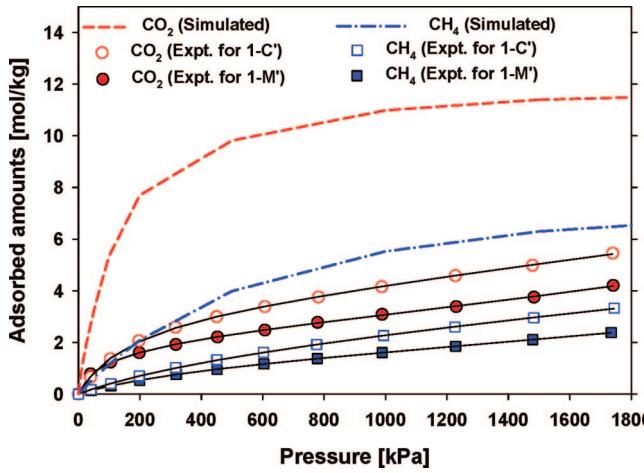

Figure 4. Comparison of experimental and simulated single-component isotherms of CO_2 and CH_4 in **1** at 296 K. The lines through the experimental data are fits to the dual-site Langmuir−Freundlich model.

3.2. Pure Gas Adsorption Isotherms. The adsorption isotherms of pure CO_2 and CH_4 on the evacuated samples **1-C′** and **1-M′** were experimentally measured up to around 18 atm at 296 K. Simultaneously, calculated adsorption isotherms for pure CO_2 and CH_4 in **1** at 296 K were obtained by GCMC simulations. Figure 4 shows the comparison between experimental and simulated single-component isotherms of CO_2 and CH_4 in **1** at room temperature. All isotherms show type I behavior, which is a typical characteristic of microporous materials. In all three cases, CO_2 is more strongly adsorbed than CH_4, which is expected because CO_2 has a significant quadrupole moment, whereas CH_4 is nonpolar. Both evacuated samples show much lower adsorption

(55) Chen, B.; Ma, S.; Zapata, F.; Lobkovsky, E. B.; Yang, J. *Inorg. Chem.* **2006**, *45*, 5718.

(56) Kondo, A.; Noguchi, H.; Carlucci, L.; Proserpio, D. M.; Ciani, G.; Kajiro, H.; Ohba, T.; Kanoh, H.; Kaneko, K. *J. Am. Chem. Soc.* **2007**, *129*, 12362.

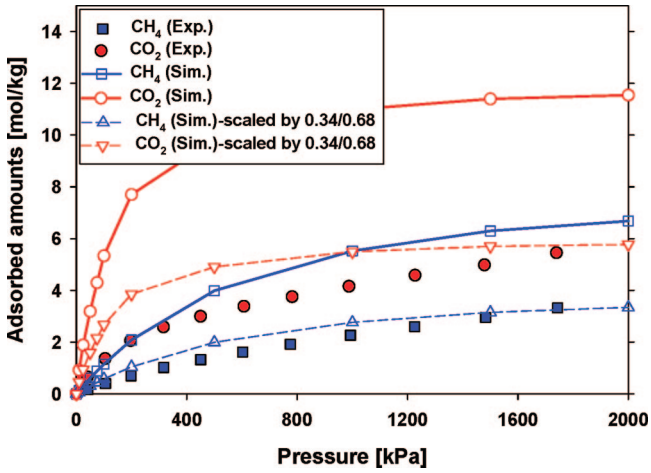

Figure 5. Comparison of experimental isotherms for **1-C′** and simulated isotherms that are scaled considering the micropore volumes in Table 1.

capacities for CO_2 and CH_4 than the simulated isotherms, and **1-C′** shows slightly larger adsorption capacities for both components than **1-M′**. The capacities show the same trends as the nitrogen micropore volumes reported in Table 1. The reduced pore volumes may be due to nonvolatile reactants in the pores, partial collapse, or more interpenetration as reasoned from the PXRD patterns for as-synthesized samples (**1-C** and **1-M**). Since the GCMC simulations have been performed for perfect crystals, these simulated isotherms overestimate the experimental data.[57] Hence, the discrepancy between the experimental and simulated isotherms is not unexpected.

From Table 1, the DR micropore volume (0.34 m^2/g) of **1-C′** calculated from the N_2 isotherm at 77 K is only half of the micropore volume (0.68 m^2/g) calculated geometrically from the crystal structure. In order to consider this difference, we applied a scaling factor (0.34/0.68 = 0.5) to the original GCMC isotherms. As represented in Figure 5, the scaled GCMC isotherms match fairly well with the experimental CO_2 and CH_4 isotherms for **1-C′**, especially in the saturation regime. Similar scaling methods have already been used in some earlier adsorption studies of MOFs.[18,57]

The DR micropore volume of **1-M′** (0.064 m^2/g) calculated from the N_2 isotherm at 77 K is much smaller compared to the micropore volume for the perfect crystal (0.68 m^2/g). However, as shown in Figure 4, the CO_2 and CH_4 isotherms of **1-M′** do not show a decrease from the simulation of this magnitude. The CO_2 and CH_4 isotherms of **1-M′** show much larger adsorption capacities than expected based on the surface area and pore volume derived from the N_2 isotherm at 77 K. In this case, the large difference between simulated and experimental isotherms cannot be solely explained by the scaling factor calculated from the N_2 isotherm at 77 K. It should be kept in mind that the nitrogen isotherms are measured at 77 K, but the CO_2 and CH_4 isotherms are at room temperature. For tightly constricted pores, it is possible that molecules cannot overcome the diffusional barriers within the crystals to fill the pores at low temperatures, whereas at higher temperatures diffusion occurs readily. This sort of behavior has been observed in other systems[58,59] and predicted theoretically.[60]

3.3. Binary Mixture Adsorption. IAST was used to predict binary mixture adsorption from the experimental pure-gas isotherms. It has been reported that IAST can accurately predict gas mixture adsorption in many zeolites[13,24,25] and more recently some MOF materials.[13,19] Although other theories exist for such predictions, IAST continues to serve as the benchmark for the prediction of mixed-gas adsorption equilibria from single-component isotherms.[13,14,19,61,62] In order to perform the integrations required by IAST, the single-component isotherms should be fitted by a proper model. There is no restriction on the choice of the model to fit the adsorption isotherm, but data over the pressure range under study should be fitted very precisely.[13,14] Several isotherm models were tested to fit the experimental pure isotherms for CO_2 and CH_4 in **1-C′** and **1-M′**, and the dual-site Langmuir−Freundlich equation was found to best fit the experimental data (see Supporting Information):

$$q = q_{m1} \cdot \frac{b_1 \cdot P^{1/n_1}}{1 + b_1 \cdot P^{1/n_1}} + q_{m2} \cdot \frac{b_2 \cdot P^{1/n_2}}{1 + b_2 \cdot P^{1/n_2}} \qquad (1)$$

Here, P is the pressure of the bulk gas at equilibrium with the adsorbed phase (kPa), q is the adsorbed amount per mass of adsorbent (mol/kg), q_{m1} and q_{m2} are the saturation capacities of sites 1 and 2 (mol/kg), b_1 and b_2 are the affinity coefficients of sites 1 and 2 (1/kPa), and n_1 and n_2 represent the deviations from an ideal homogeneous surface. Figure 4 shows that the dual-site Langmuir−Freundlich equation fits the single-component isotherms extremely well. The R^2 values for all the fitted isotherms were over 0.99995. Hence, the fitted isotherm parameters were applied to perform the necessary integrations in IAST.

Adsorption isotherms predicted by IAST for equimolar mixtures of CO_2/CH_4 in **1-C′** and **1-M′** as a function of total bulk pressure are shown in Figure 6a,b, respectively. For both samples, CO_2 is preferentially adsorbed over CH_4 because of stronger interactions between CO_2 and the MOF. The presence of methane does not significantly affect the adsorption of CO_2, but methane adsorption is much lower in the mixtures than in single-component adsorption because of competition from CO_2, which adsorbs more strongly. Figure 6a,b also presents the predicted selectivity for CO_2 over CH_4 for the two samples. The selectivity $S_{A/B}$ in a binary mixture of components A and B is defined as $(x_A/y_A)/(x_B/y_B)$, where x_i and y_i are the mole fractions of component i (i = A,B) in the adsorbed and bulk phases, respectively. Note that in the Henry regime $S_{A/B}$ is identical to the ratio of the Henry constants of the two species. In the low-pressure region, the selectivity of **1-M′** is extremely large, ∼30, and the selectivity drops as pressure increases. Sample **1-C′** is also modestly selective for CO_2 over methane, and the selectivity shows only a weak pressure dependence. The different behavior in the two materials is likely due to subtle differences in the MOF structures. For both **1-C′** and **1-M′** at very low pressures, the ratio of the CO_2 and CH_4 Henry constants is very close to the selectivity, as expected. This serves as a consistency test of the IAST calculations. The selectivities of **1-C′** and **1-M′** are similar in the high-pressure regime, as interactions between guest molecules

(57) Dubbeldam, D.; Frost, H.; Walton, K. S.; Snurr, R. Q. *Fluid Phase Equilib.* **2007**, *261*, 152.
(58) Garrido, J.; Linares-Solano, A.; Martin-Martinez, J. M.; Molina-Sabio, M.; Rodriguez-Reinoso, F.; Torregrosa, R. *Langmuir* **1987**, *3*, 76.
(59) Lozano-Castello, D.; Cazorla-Amoros, D.; Linares-Solano, A. *Carbon* **2004**, *42*, 1233.
(60) Nguyen, T. X.; Bhatia, S. K. *J. Phys. Chem. C* **2007**, *111*, 2212.
(61) Murthi, M.; Snurr, R. Q. *Langmuir* **2004**, *20*, 2489.
(62) Wu, J. Q.; Zhou, L.; Sun, Y.; Su, W.; Zhou, Y. P. *AIChE J.* **2007**, *53*, 1178.

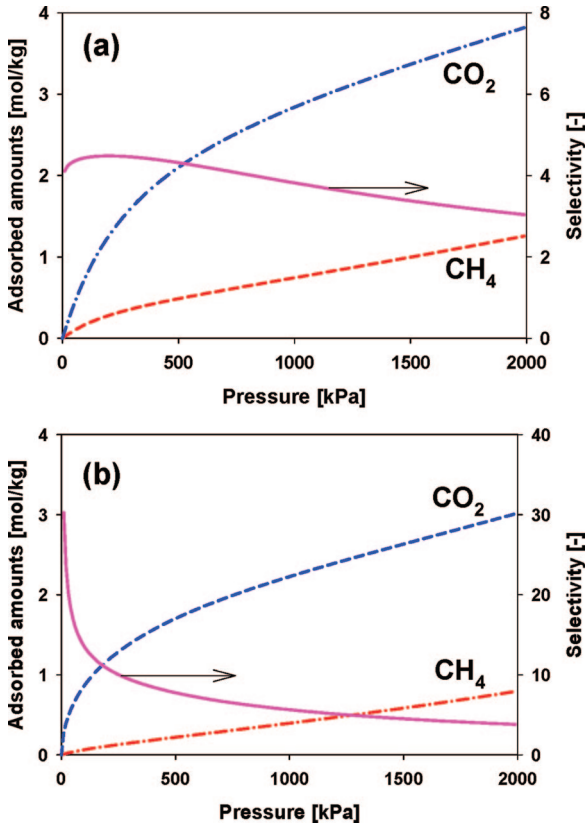

Figure 6. The IAST-predicted isotherms and selectivities of equimolar mixtures of CO_2 and CH_4 in (a) **1-C′** and (b) **1-M′** at 296 K as a function of the (total) pressure.

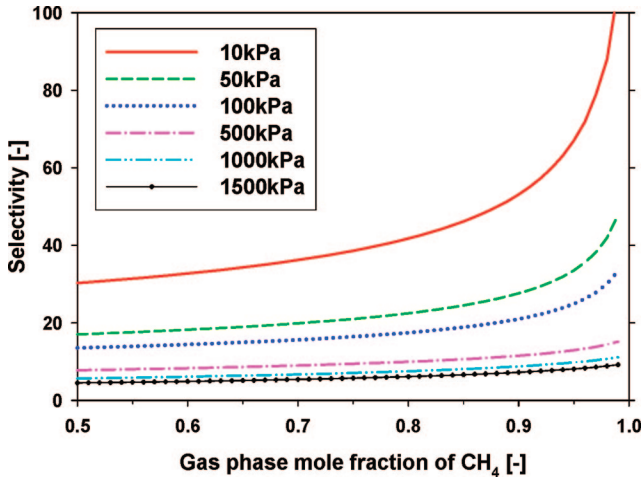

Figure 7. The IAST predicted selectivities at different mixture compositions and different pressures for **1-M′** at 296 K.

become more important compared to the interactions with the framework.

The IAST-predicted selectivities at different mixture compositions and different pressures for **1-M′** are shown in Figure 7. The selectivity increases rapidly as the gas-phase mole fraction of CH_4 approaches unity. At $y_{CH4} = 0.95$, a typical feed composition for natural gas purification, extremely high selectivities (8−67) are obtained. Even at $y_{CH4} = 0.5$, the selectivity is in the range of 4−30, among the highest selectivities reported. This is much higher than the selectivities reported for other MOFs from GCMC simulations: Cu-BTC (6−10)[19,20] and MOF-5 (2−3).[13,19] The CO_2/CH_4 selectivities reported for zeolite 13X[2] and zeolite β[6] are 2−24 and 28, respectively, at similar conditions. These results

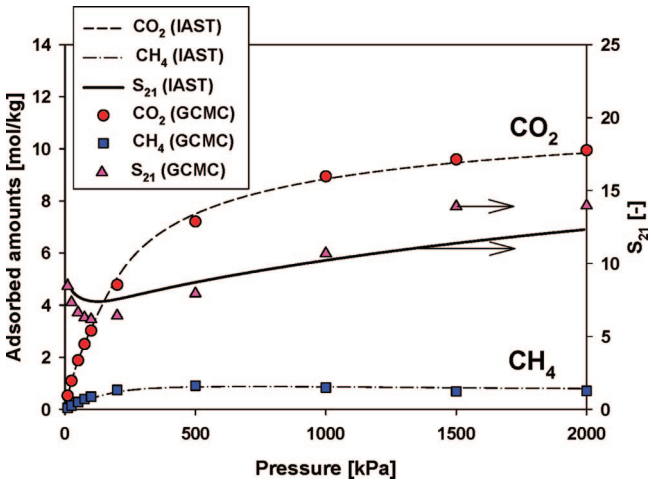

Figure 8. Verification of the IAST calculations by GCMC simulations for equimolar mixtures of CO_2 and CH_4 in **1** at 296 K. The IAST calculation was based on single-component GCMC isotherms (excess adsorbed amounts). Also, the GCMC mixture isotherms represent the excess adsorbed amounts.[63]

suggest that **1-M′** is a promising candidate for natural gas purification, and also a good candidate for CO_2 separation from other CO_2/CH_4 mixtures. Separation processes at low pressures, such as vacuum swing adsorption (VSA), could be extremely efficient using **1-M′** because the selectivity increases dramatically with decreasing pressure. Very high selectivity can be obtained even at 1−5 atm, which are the typical pressures in PSA processes.

3.4. Verification of the IAST Model by GCMC Simulations. The mixture results in Figures 6 and 7 were obtained from single-component experimental isotherms using IAST. As the name implies, IAST assumes an ideal adsorbed phase with activity coefficients of unity for all components. IAST usually works well at low loading—it is exact in the Henry's law region—and often works at higher loadings, too. Unfortunately, it is difficult to say when IAST will work and when it will fail.[61] To test the applicability of IAST for the mixed-ligand MOF **1**, we turned to GCMC simulation. First, GCMC single-component isotherms (excess adsorbed amounts) of CO_2 and CH_4 in **1** at 296 K were fed into IAST to predict the adsorption of equimolar mixtures of CO_2 and CH_4 in **1**. Then, GCMC simulations were performed for the mixtures at the same conditions. As shown in Figure 8, the IAST-predicted mixture isotherms match very well with the GCMC mixture simulation results (excess adsorbed amounts). The selectivity is also predicted well by IAST for this system, although slight deviations are observed in the high pressure regime. In addition, the ratio of Henry constants of CO_2 and CH_4 is very close to the IAST selectivity at zero pressure as required. The excellent agreement between the GCMC mixture adsorption isotherms and the IAST results validates the use of IAST for this system and strengthens the conclusion that **1**, and in particular **1-M′**, is a strong candidate for the separation of CO_2 from CH_4 gas streams.

4. Conclusions

We have synthesized a mixed-ligand MOF ($Zn_2(NDC)_2(DPNI)$, **1**, by two different methods, the conventional method (**1-C**) and a new microwave-assisted method (**1-M**). The evacuated sample **1-M′** shows slightly lower capacity for CO_2 and CH_4 than **1-C′**, but it has much higher selectivity of CO_2 over CH_4, based upon the IAST analysis of the single-component isotherms. This is

(63) Sircar, S. *J. Chem. Soc., Faraday Trans. 1* **1985**, *81*, 1527.

among the highest selectivities reported for CO_2 and methane. The applicability of IAST was verified by GCMC simulations of the binary mixture adsorption. These results suggest that **1-M′** is promising for CO_2/CH_4 separations, especially for natural gas purification.

Acknowledgment. This work was supported by the Korea Research Foundation Grant funded by the Korean Government (MOEHRD) (KRF-2006-352-D00040), and by the U.S. Department of Energy (DEFG02-1ER15244 and DEFG02-03ER15457). K.L.M. gratefully acknowledges a Laboratory-Grad fellowship from Argonne National Laboratory.

Supporting Information Available: Details of volumetric adsorption measurements, additional characterization results, isotherm fitting results, and potential parameters for the GCMC simulations. This material is available free of charge via the Internet at http://pubs.acs.org.

LA800555X